Enhancement of selective photocatalytic conversion of guaiacol to add-value products by β-cyclodextrin macromolecules anchored to α-Fe_2O_3/TiO_2

Nicole Espinoza [a,b], Susana Rojas [a,b], David Contreras [b,d,e], Nestor Escalona [a,b,c,f,g], Ricardo Salazar [c], Elizabeth Vergara , Miguel Angel Laguna[i], Lorena Barrientos [a,b,g*]

[a] *Facultad de Química y de Farmacia, Pontificia Universidad Católica de Chile, Vicuña Mackenna 4860, Macul, Santiago, Chile.*

[b] *Millennium Nuclei on Catalytic Processes Towards Sustainable Chemistry (CSC), Chile*

[c] *Facultad de Química y Biología, Universidad de Santiago de Chile, Avenida Libertador Bernardo O'Higgins 3363, Estación Central, Santiago, Chile*

[d] *Renewable Resources Laboratory, Biotechnology Center, University of Concepción, University Campus, Concepción, Chile*

[e] *Faculty of Chemical Sciences, University of Concepción, University Campus, Concepción, Chile*

[f] *Chemical Engineering and Bioprocesses, School of Engineering, Pontificia Universidad Católica de Chile, Vicuña Mackenna 4860, Macul, Santiago, Chile*

[g] *Research Center for Nanotechnology and Advanced Materials CIEN-UC, Pontificia Universidad Católica de Chile, Chile*

[i] *Instituto de Ciencia de Materiales de Aragon, CSIC-Universidad de Zaragoza, Campus Río Ebro, 50018 Zaragoza, Spain*

Corresponding Author

*Dr Lorena Barrientos

e-mail: lbarrientop@uc.cl

Phone: +56 22 354 7556

Abstract

Biomass is a naturally abundant, sustainable, and clean resource, which has the potential to replace fossil feedstock for sustainable production of high added-value chemicals. However, an efficient conversion process is still difficult to be achieved due to the hard reaction conditions. In this study as a novel and versatile macromolecule was used to this propose, the selective conversion of guaiacol was evaluated using 0.2, 1.0, and 2.0 molar ratio of β-cyclodextrin (β-CD) anchored on 0.7 wt% α-Fe_2O_3/TiO_2 under mild conditions reaction. 1.0 molar ratio of β-CD promoted photo-oxidation of guaiacol produced mainly *p*-benzoquinone with ~68% selectivity at ~10% conversion. To understands this effect, Electron Paramagnetic Resonance Spectroscopy (EPR) in *operando* mode and Diffuse Reflectance Spectroscopy (DRS) experiments were performed. The results show that 1.0 molar ratio of β-CD decreases the bandgap from 3.06 to 2.76 eV, controlling the ·OH radical concentration due to the formation of a covalent bond between β-CD and semiconductors, improving the adsorption capacity of guaiacol over the surface of photocatalyst, resulting on the enhancement of photochemical behavior in terms of activity and selectivity. Additionally, a possible pathway of guaiacol oxidation was proposed through the oxidation intermediates. Furthermore, the photocatalyst β-CD/α-Fe_2O_3/TiO_2 can be recycled efficiently and reused three times, without loss in reactivity.

1. Introduction

Organics obtained from fossil fuels are used in medicines, lubricants, paints, solvents, and even in food [1]. However, technologies employed by several industries generally require drastic experimental conditions such as the presence of harmful oxidizing agents, toxic solvents, and high temperatures and pressures [2]. Currently, the search for renewable and clean alternatives for the obtention of several products is attracting more attention. In this sense, the use of lignocellulosic biomass for the efficient transformation into chemical and high added-value products is being researched [3]. Lignin is one of the three main subcomponents of lignocellulosic biomass in terrestrial ecosystems and makes up nearly 30% of the organic carbon sequestered in the biosphere [4]. As a result of its rich content of aromatic carbon, lignin has the potential to be decomposed to yield valuable chemicals and alternatives to fossil fuels [5]·[6]. The selective oxidation of guaiacol to several molecules is an attractive reaction in the biomass conversion field because guaiacol comes from lignin and remains stable in the wood waste of the pulp and paper industry [7]. However, improving the selectivity of the photocatalyst to avoid mineralization of the organic molecules obtained is a key challenge. In this

sense, few works have reported the degradation of guaiacol to carboxylic acids or mineralization and not promote the selective oxidation to aromatic organics [8]–[10].

Diverse technologies have been developed to replace strong and polluting reaction conditions, among them heterogeneous photocatalysis has gain attention. This technology is universally recognized as “green” and inexpensive because it can be carried out under mild conditions reactions and photocatalytic reactions do not generate toxic by-products [3], [12], [13]. Currently, it is known that the formation of a heterojunction between TiO_2 and α-Fe_2O_3 improves the absorption of solar radiation and increases the photocatalytic activity of the new material [14]. However, this nanocomposite is mainly used to take advantage of the photocatalytic degradation rate of several molecules, thus avoiding selectivity for added-value molecules [15]–[19]. From this perspective, the use of β-cyclodextrin (β-CD), a low-cost oligosaccharide formed by glucopyranose units, linked by α-1,4-glucosidic (C-O-C) bonds with free electrons that generate high electronic density must be noted [20]. This characteristic, together with the hydrophobicity of the internal cavity, enables insoluble or poorly soluble molecules to capture a wide variety of organic compounds. Furthermore, β-CD does not only alter the external morphology of the material but also some of its intrinsic properties, such as photoactivity, photoelectric activity, and energy transfer, among others[21]–[24]. The use of β-CD on photocatalytic reaction improves the conversion of the analyte and promotes the selective oxidation of aromatic compounds due to the generation of molecular recognition sites on photocatalyst surface [25]–[28]

In this work, for the first time as a versatile novel concept, the use of β-CD macromolecule as a selective agent in the photocatalytic process was achieved. Different β-CD molar ratio anchored over 0.7 wt% α-Fe_2O_3/TiO_2 (β-CD/α-Fe_2O_3/TiO_2) composite, was synthesized by in situ preparation of 0.7 wt% α-Fe_2O_3 over commercial TiO_2 and the subsequent anchoring of β-CD in aqueous media and under mild conditions reactions. Subsequently, as obtained photocatalysts were used for the selective conversion of guaiacol as a lignin model compound in aqueous media, under UVA-Visible light.

2. Experimental

2.1 Materials

Iron (III) nitrate nonahydrate ($Fe(NO_3)_3 \cdot 9H_2O$, ≥99.8%), Titanium(IV) oxide, anatase (TiO_2, < 25 nm, 99.7%), Sodium carbonate anhydrous (Na_2CO_3, ≥99.5%) and β-Cyclodextrin (β-CD, ≥97%) were purchased from Sigma-Aldrich and Merck, and used as received. Deionized water was used in all experiments.

2.2 Preparation of α-Fe_2O_3/TiO_2 nanomaterials

The ultrasonic-assisted co-precipitation method was employed to prepare α-Fe_2O_3/TiO_2 nanoparticles [15]. Titanium dioxide (anatase, ~25 nm) and Iron (III) nitrate nonahydrate ($Fe(NO_3)_3 \cdot 9H_2O$) were used as precursors for the preparation of α-Fe_2O_3/TiO_2 powders. For the 0.7 wt% TiO_2 decorated with α-Fe_2O_3, a suspension of TiO_2 nanoparticles at pH 7 was added into a solution containing 0.55 g of Na_2CO_3 dissolved in 200 ml deionized water under ultrasonication at 80°C. Then, 0.25 g of $Fe(NO_3)_3 \cdot 9H_2O$ were dissolved in deionized water and added to the solution drop-wise using ultrasonication for about 2 h. Finally, the 0.7 wt% TiO_2 decorated with α-Fe_2O_3 nanoparticles were collected and washed several times with deionized water and dried in an oven at 100°C for 12 h.

2.3 Preparation of β-CD/α-Fe_2O_3/TiO_2 nanomaterials

A saturated solution of β-CD an aqueous medium was prepared. For the 0.7 wt% β-CD/α-Fe_2O_3/TiO_2 (0.2 mol) sample, 1 g of β-CD was introduced into a solution containing 0.4 g of α-Fe_2O_3/TiO_2 dissolved in 330 ml deionized water under ultrasonication at 48°C for 1 h. After the mixture reacted, the solution was stirred for about 24 h in a completely dark room at ambient temperature. Finally, the β-CD/α-Fe_2O_3/TiO_2 nanoparticles were collected and washed several times with deionized water and ethanol and dried later in an oven at 100°C. Similarly, β-CD/α-Fe_2O_3/TiO_2 nanoparticles were also synthesized with other proportions of β-CD. Samples of α-Fe_2O_3/TiO_2 were decorated with β-CD in proportions such as 0.0, 0.2, 1.0, 2.0 mol (FT, FT:CD1, FT:CD2, FT:CD3, respectively), in which the photocatalyst weight was kept constant.

2.4 Characterization of α-Fe_2O_3/TiO_2 and β-CD/α-Fe_2O_3/TiO_2

X-ray photoelectron spectroscopy (XPS) (Staib Instruments) was equipped with a DESA 150 electron spectrometer and RQ-300 x-ray source with an Al source radiation (1486.6 eV) was used to analyze bonding information of the α-Fe_2O_3/TiO_2 nanomaterial. The detailed XPS regions were analyzed and fitted using Gaussian and Lorentzian function products. Shirley backgrounds and source satellites were subtracted from spectra. Data treatment was performed with the help of CasaXPS software version 2.3.16. X-ray diffraction (XRD) patterns were recorded at room temperature on a Bruker D-8 diffractometer using CuKα (λ = 1.5418˚A) radiation as the X-ray source. Diffraction patterns were measured using a Bragg-Brentano geometry configuration with a rotating sample holder for powder samples. An angular step of 0.02° with a time of 1 second was employed in the 10° to 80° whole range. Phase identification and Rietveld refinement analysis were carried using MAUD software and the Crystallography Open Database (COD) [29]. The average

(1)

crystallite size in each powdered nanocomposite was estimated with Scherrer's equation (calculated from the line broadening of the {101} peak) with the eqn.1:

$$B(2\theta) = K \cdot \lambda / L \cos \theta$$

where the peak width, B(2θ), at a particular value of 2θ (θ being the diffraction angle, λ the X-ray wavelength) is inversely proportional to the crystallite size L; the constant K is a function of the crystallite shape but is generally taken as being about 1.0 for spherical particles.

The morphology, crystallography, and particle size of the materials were examined using High-resolution transmission electron microscopy (HRTEM) using a JEOL 2000FX TEM microscope at 200 kV . Furthermore, the composition of photocatalyst surface was determined in a field emission scanning electron microscope (FESEM), using a QUANTA 250 FEG from FEI Thermo Fisher Scientific coupled with an energy dispersive X-Ray spectroscopy system (EDS). Micrographs were obtained under an accelerating voltage of 10 kV, employing secondary and backscattered electron detectors.

The FT-IR spectra were analyzed to identify the presence of β-CD over the surface of α-Fe_2O_3/TiO_2 which were recorded in the range 4000–400 cm^{-1} on an FT-IR spectrometer (Jasco, FT-IR/4600) using the KBr pellet technique.

The N_2 adsorption-desorption isotherms were measured at 77 K in a Micrometrics Instrument Corporation 3 Flex-MS volumetric adsorption analyzer. The specific surface area was calculated through the Brunauer– Emmett–Teller (BET) method and the external surface area was defined using the *t-plot* method. UV–vis diffuse reflectance spectra were recorded on a Shimadzu 2600 UV–vis spectrophotometer equipped with ISR-2600 Plus integrating sphere, with $BaSO_4$ as the background between 200 and 800 nm. The bandgap of the samples is calculated by interpolating the graph of the transformed Tauc function versus the energy of the light absorbed by the nanocomposite [30], shown in eqn (2):

$$\alpha = A(h\nu - Eg)^{(1/n)} / h\nu \qquad (2)$$

where α is the absorption coefficient, Eg is the bandgap energy (eV), A is a proportional constant, the value of the exponent represents the character of the electronic transition, whether direct or indirect: n is 0.5 for direct band gap materials or 2 for indirect band gap materials. Both TiO_2 and Fe_2O_3 is well known to have an indirect band gap [31].

To determine the role of β-CD in the formation of hydroxyl radicals during the oxidation of guaiacol on the photoactivated surface of the nanocomposite, in situ electron paramagnetic resonance (EPR) measurements were performed with an

EMX micro 6/1 Bruker ESR spectrometer working at the X-band, equipped with a Bruker Super High QE cavity resonator, and using 5,5-Dimethyl-1-pyrroline *N*-oxide (DMPO) as a spin trap in aqueous media. The reaction was initiated by turning on the irradiation source and carried out in an EPR sample tube (ER 221TUB/, 4mm I.D.) inside the EPR cavity, which was irradiated in the UVA-Visible region. The in-situ measurement was performed at room temperature. Typical instrumental conditions were center field, 3514 G; sweep width, 200 G; microwave power, 20 dB; modulation frequency, 100 kHz; time constant, 0.01 ms; sweep time, 30 s; modulation amplitude, 1.00 G; and receiver gain, 30 dB.

2.5 Photocatalytic conversion of guaiacol

The photocatalytic activity of α-Fe_2O_3/TiO_2 and β-CD/α-Fe_2O_3/TiO_2 nanocomposites with different β-CD content was assessed using the photoconversion of aqueous solution of guaiacol under a 35W Xe arc lamp (380-1300 nm with a relatively smooth emission curve from region UV to visible). The absorption spectrum of the lamp was recorded with a fluorescence spectrometer (LS–45, PerkinElmer) in luminescence mode and the spectrum is shown in Fig. S1.

The photocatalysis was carried out in a cylindrical photoreactor of 280 mL of capacity and with a refrigeration system (Fig. S2). The temperatures inside the photocatalytic reactor reached 25 ± 2 °C. The solution of 280 mL deionized water has added guaiacol (0.4 mM) and 1 g/L of catalyst. The suspension was stirred for 1h in the dark until reaching the adsorption-desorption equilibrium. At specific time intervals (each 60 min), 2 mL samples were taken out and centrifuged to remove the photocatalyst.

The intermediates obtained of the photocatalysis were monitored using high-performance liquid chromatography (HPLC; Shimadzu, LC-20 VP prominence pump and SPD-20A UV–visible detector adjustable to 200 and 800 nm with reverse-phase ODS column). The Purospher Star RP-18 column was obtained from Merck and has the next characteristic 150 mm × 4.6 mm, 5 µm particle size and worked at 25°C. The mobile phase was composed of acetonitrile and triple distilled water that contained 0.1% formic acid in a 25:75 ratio v/v, respectively. Products obtained were identified and quantified by the standard addition method.

3. Results and discussion

Characterization of the photocatalysts

To determine the amount of iron species, XPS high-resolution spectra were measured (Fig.1). Peaks corresponding to Ti^{4+} assigned to Ti $2p_{3/2}$ and Ti $2p_{1/2}$ were observed at 458.3 eV and 464.0 eV, respectively. Peaks corresponding to Fe^{3+} for Fe $2p_{3/2}$ and Fe $2p_{1/2}$ were observed at 710.3 eV and 723.5 eV, respectively,

indicating that iron in FT sample is probably α-Fe_2O_3 and fulfills our purpose. On the other hand, the oxygen 1s signal shows contributions due to metal oxides, carbon, and water present in the photocatalyst. The molar ratio obtained for Fe/Ti is 0.643 which is consistent with the preparation method.

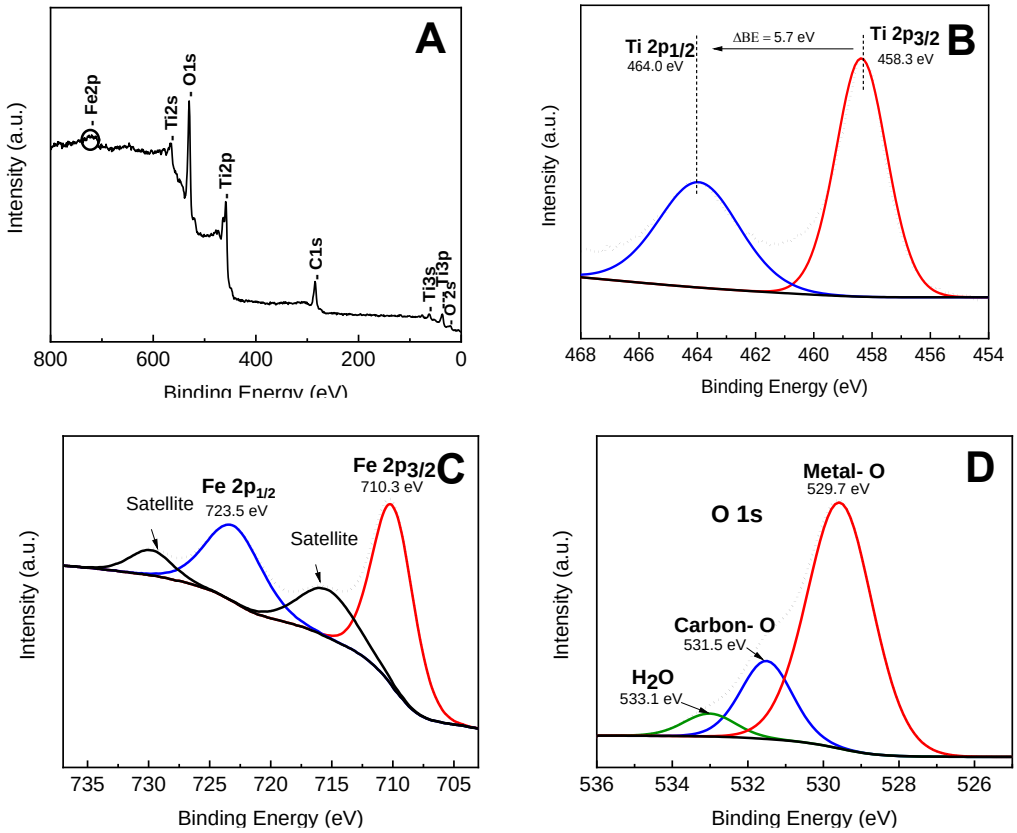

Fig. 1 XPS spectra of FT: A) survey spectrum, high resolution measurements for B) Ti 2p, C) Fe 2p, D) O 1s emission lines.

XRD patterns were recorded to investigate the crystal structure, phase purity, and particle size of FT and FT:CD2 samples which are shown in Fig.2. Several crystalline peaks were detected for the TiO_2 sample, where the predominant is (101) plane. These results indicated the existence of anatase in the surface of the nanomaterial (peaks leveled with black circles) [32], [33]. Additional diffraction peaks observed (labeled with blank circles) correspond to the presence of the rutile phase[34], [35]. On the other hand, β-CD attachment over the surface α-Fe_2O_3/TiO_2 does not modify the crystalline structure or the purity of the semiconductor since the peaks remain unchanged. Crystal planes related to α-Fe_2O_3 were not observed probably to the low concentration and small particle sizes of the samples.

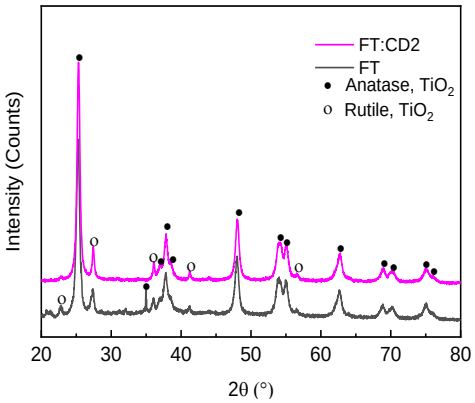

Fig. 2 XRD patterns of 0.7 wt% α-Fe_2O_3 over TiO_2 synthesized and 1.0 mol β-CD attachment.

HRTEM analysis was used to examine the particle size and crystallinity photocatalysts. HRTEM micrographs of FT sample is shown in Fig. 3A and insets. It is observed agglomerated and fused α-Fe_2O_3 and TiO_2 nanoparticles in the range of 4- 8 nm and 10-14 nm with a main diameter of 6 ± 2 nm and 12 ± 1 nm, respectively. Likelly that results are atributed to the TiO_2 nature which remain such as is comercialized where α-Fe_2O_3 is formed in situ over its surface. Meanwhile, FT:CD2 of the nanocomposite α-Fe_2O_3/TiO_2 with crystals mainly in the range of 4-12 nm with a main diameter of 8 ± 2 nm (Fig. 3B and insets). On the other hand, the amorphous and crystalline phase of α-Fe_2O_3/TiO_2 in the FT and FT:CD2 sample can also be observed by phase-contrast image in Fig. 3C-D. The results present crystal lattice plane with the lattice fringes of 0.351 nm corresponding to the (101) the most stable thermodynamical crystal plane of anatase TiO_2 (0.44 J/m^2) in good agreement with XRD difraction patern discused above [36]. The fringe spacing of ~0.488 nm also matches with the spacing of the (111) crystal planes of the α-Fe_2O_3 corresponding to the predominant phase in hematite structure. Furthermore, it is shown the formation of heterojunction between α-Fe_2O_3 and TiO_2 corresponding to grain limit. Besides, the successful loading of α-Fe_2O_3 over TiO_2 is confirmed by EDS analysis (Fig. S3), which shows the presence of Fe, Ti, O, and C peaks, indicating that the molar ratio is 0.67 wt% α-Fe_2O_3/TiO_2 and therefore consistent with the XPS and HRTEM analysis.

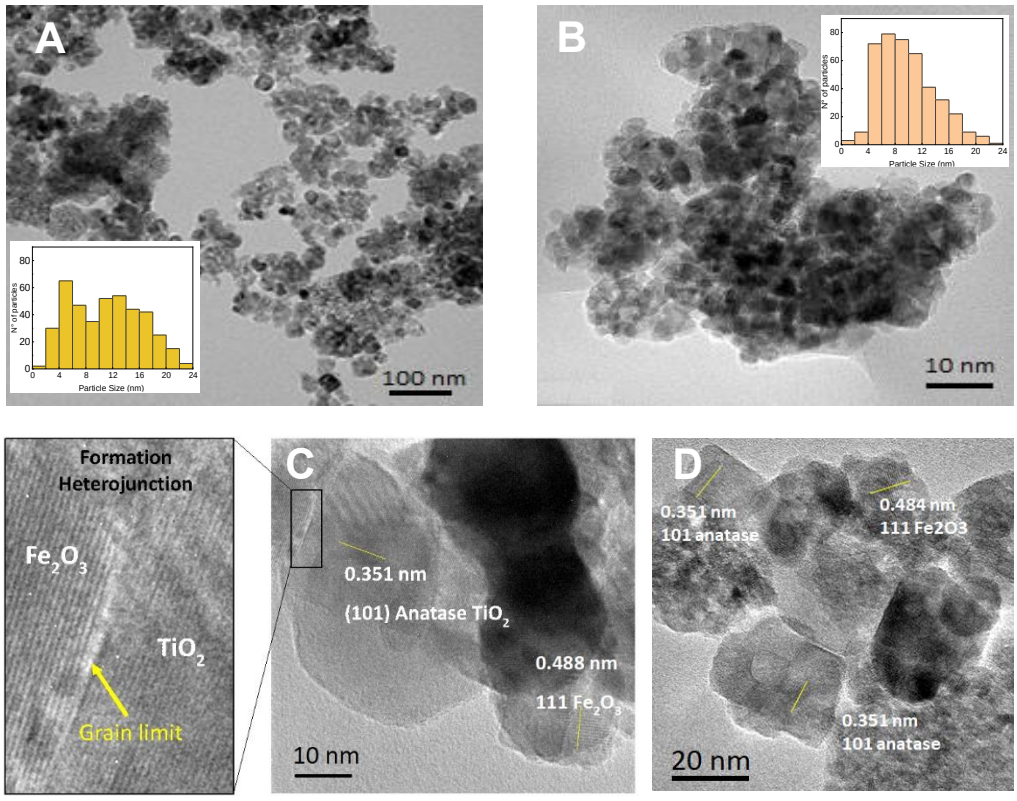

Fig. 3 HRTEM micrographs of A) FT and B) FT:CD2, respectively. Increasing magnification micrograph of C) FT and D) FT:CD2.

The modification of α-Fe_2O_3/TiO_2 surface with β-CD has been characterized using FT-IR in order to evaluate whether the chemical reaction successfully produced the anchoring of β-CD on the nanocomposite, see Fig.4. The peak at 3388 cm^{-1} is related to the stretching and bending vibrations of the O—H groups, attributed to hydroxyl groups of β-CD and the cross-linking bonds, as well as assigned to water molecules in the β-CD cavities [37]. The stretching vibration peak of the C—H bond appears at 2924 cm^{-1} and proves that the structure of β-CD has not been damaged [38]. Asymmetric and symmetric C—O—C stretching can be seen at 1159 cm^{-1} and 945 cm^{-1}, respectively corresponding to breath of ring. The high-intensity absorption peaks at 1645 cm^{-1} and 1419 cm^{-1} are assigned to the bending mode of adsorbed water molecules. Besides, the displacement of the observed peak at 1612 cm^{-1} for FT implies that the β-CD anchored on the surface of the photocatalyst is forming a covalent bond corresponding to the vibration between M—OH [39]. When the molar ratio of β-CD increases, this bond becomes weaker attributed to less interaction between them.

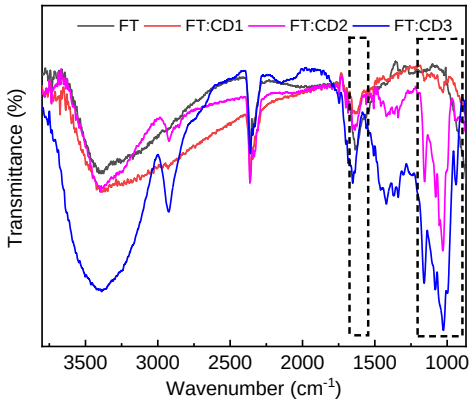

Fig.4 FT-IR spectra of α-Fe_2O_3/TiO_2 modified with β-CD attachment in different molar ratio.

The Diffuse Reflectance Spectroscopy (DRS) of FT, FT:CD1, FT:CD2, FT:CD3 provides information about the optical properties of the photocatalysts. The observed DRS spectra of the sample are summarized in Table 1 and shown in Fig.S3. Titanium dioxide decorated with 0.7 wt% hematite showed a slight shift towards visible radiation absorption, indicating the formation of a heterojunction between both semiconductors as reported for HRTEM analysis [40]. The incorporation of β-CD in FT:CD1 and FT:CD2 promotes bandgap reduction through the formation of an interaction between the hydroxyl groups of β-CD and FT, improving the light absorbance in the visible region by the nanocomposite [41]. This behavior was explained for Wonyong Choi and co-workers [81], which was attributed to the formation of charge-transfer complex between them due to a large amount of electro-donors groups in the macromolecule. However, an excess of β-CD in the nanocomposite causes an increase in bandgap that could be attributed to the absorption of β-CD in the UV region , which contributes to a slight run of the TiO_2 band at shorter wavelengths [42].

Table 1

Resume results obtained for photocatalyst samples at different molar ratios of β-CD 0.0 to 2.0 over α-Fe_2O_3/TiO_2.

Photocatalyst	S_{BET} (m^2/g)	Average pore diameter (nm)	Band gap (eV)	Band edge (nm)	XPS binding energies of main peaks (eV)		Fe/Ti atomic ratio
					Ti 2p	Fe2p	
FT	107	10	3.06	405			
FT:CD1	25	38	2.77	448	458.3	719.9	0.643
FT:CD2	7	29	2.76	449			
FT:CD3	3	10	3.06	405			

The nitrogen adsorption-desorption isotherms of the photocatalysts are depicted in Fig.S4. The specific surface area and average pore diameter is presented in Table 1. The presence of β-CD causes a noticeable change in specific surface area of nanomaterial by decreasing its value when increasing its molar ratio. This effect could be explained by the possible formation of carbon from cyclodextrin dehydration at the surface of photocatalyst blocking up the pores [43]. The increase in the β-CD molar ratio anchored to the nanocomposite causes the isotherm to change from Type IV with a hysteresis cycle H2 to a Type III isotherm without a hysteresis cycle when its value increases [44]. These changes suggest that the nanocomposite without β-CD exhibits a narrow range of uniform mesopores. The smallest pores present in the material are blocked by the presence of β-CD, so the surface of the material decreases [45].

Photocatalytic activity

Fig.5A shows the normalized conversion of guaiacol with different β-CD molar ratios over α-Fe_2O_3/TiO_2 and photolysis reference. The normalized conversion of guaiacol for FT after 300 min of irradiation was 56%. Meanwhile, it was found that the variation of the β-CD molar ratio over the α-Fe_2O_3/TiO_2 decrease the conversion of guaiacol during photocatalysis. Furthermore, the kinetics constant of pseudo-first order reaction for FT is four times bigger that contain β-CD (Table 2). These results indicate that the loading of β-CD played an important role in the conversion of guaiacol likely due to the less availability of ·OH radical over the surface of photocatalyst which is known as a highly reactive and non-selective reactive oxygen species (ROS). The lower amount of ·OH avoided the fast and non-selective degradation or mineralization and increased selectivity of photocatalytic reaction as shown in Table 2 [46], [47]. For better understanding of this effect, the EPR analysis was performed in an operando mode with UVA-visible light and the results are shown in Fig.5B. The results indicated that when a solution containing FT and guaiacol is irradiated, a quartet signal characteristic of the DMPO-OH adduct with a hyperfine coupling constant of 15G is observed [48]–[50]. However, the irradiation of FT:CD2 with guaiacol shows a much weaker signal for the characteristic DMPO-OH adduct with a low noise to signal ratio, indicating a considerably lower production of ·OH radical. These results indicate a high activity of the nanocomposite FT in the production of ·OH which is avoided when β-CD is attached over the surface of the semiconductor due to formation of ligand-to-metal charge transfer (LMCT) between β-CD-O-Metal. [51], [52]. These effects could be improving the selective oxidation of guaiacol by decreasing the available of ·OH radical and favor the oxygen reduction and formation of $O_2^{\cdot-}$ [53].

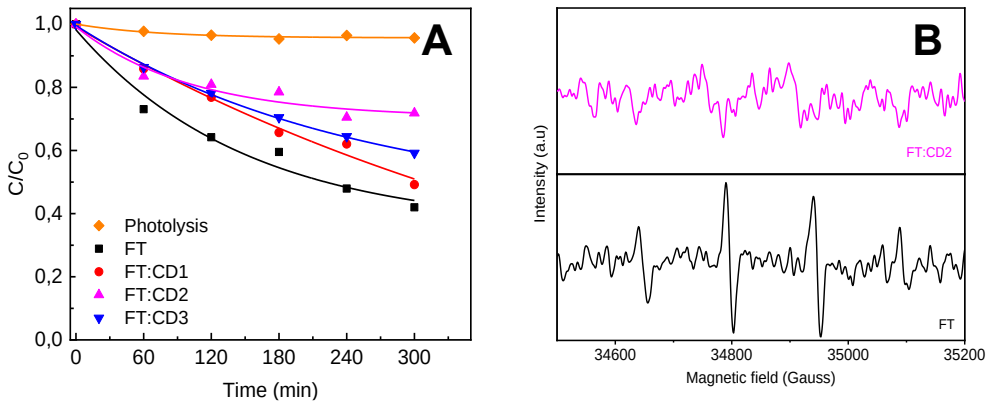

Fig. 4 A) normalized conversion of guaiacol over FT and different β-CD molar ratios over nanocomposite. Reaction conditions: $[guaiacol]_0$= 50 mg/L, $[photocatalyst]_0$= 1 g/L, B) EPR spectra of DMPO-OH adducts recorded in 5 min for FT:CD2 (pink line) and FT (black line).

The role of β-CD was investigated by examining the product distribution with the variation of macromolecule molar ratio over α-Fe_2O_3/TiO_2. The product distribution was obtained of 8.4% conversion of guaiacol for all systems in the study. The results are shown in Fig.6A-B and Table 2. The different attachment β-CD molar ratios over α-Fe_2O_3/TiO_2 increase the production of *p*-benzoquinone (A1) in comparison with FT with a selectivity four times bigger. Products intermediaries are identified as catechol (> 1%), pyrogallol (> 2%), vanillin (> 1%), syringol (0.2%), and unknow intermediaries. *p*-benzoquinone was the principal product detected in all the photocatalytic systems. However, the better systems were attributed to photocatalysts that include β-CD. This effect could be due to that *p*-benzoquinone have lower affinity for the β-CD cavity in comparison with guaiacol or other products which allows a quick release to the aqueous medium promoting greater selectivity for the inclusion of guaiacol [54]. It was supported by G. Astray and co-workers [55], indicated that the partition coefficient (P) and molar volume (Vm) likely affect the force that drives for host-guest complex formation to occur. In consequence, the minor value of hydrophobicity (LogP) and greater Vm could avoid that the inclusion complex remains stable. Furthermore, *p*-benzoquinone show the lowest value for LogP and the higher value for Vm compared to other products [56]. In this sense, the photocatalyst more selective to produce *p*-benzoquinone was FT:CD2 due to its specific amount of β-CD, morphology characteristics and lower BG absorption.

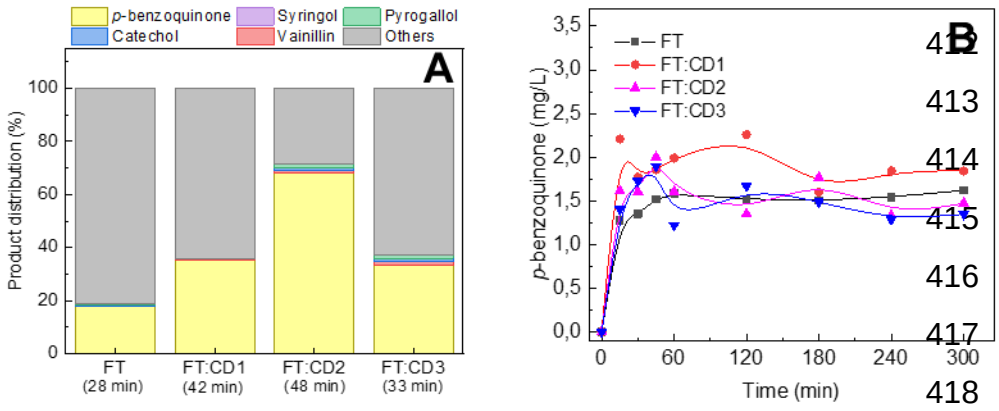

Fig. 5 A) Products distribution (%) calculated at 8.4 % of conversion of guaiacol with different β-CD molar ratios over α-Fe_2O_3/TiO_2, B) kinetic production of *p*-benzoquinone during 300 min of reaction with FT, FT:CD1, FT:CD2, FT:CD3.

Table 2

Kinetic constant of pseudo-first-order reaction, *p*-benzoquinone selectivity to 8.4% of guaiacol conversion, and amount of *p*-benzoquinone produced in the same selectivity for each photocatalyst.

Photocatalyst	k_{app} (s^{-1})	*p*-benzoquinone selectivity (%)	*p*-benzoquinone (mg/L)
FT	0.79	17.7	1.36
FT:CD1	0.19	35.1	1.82
FT:CD2	0.20	67.9	1.84
FT:CD3	0.15	33.3	1.75

Photocatalyst recyclability is important for industrial applications. As the FT:CD2 is the photocatalyst that has the best photocatalytic activity in terms of selectivity and conversion it was selected for the recyclability test. Results are shown in Fig.7. FT:CD2 was recovered using a centrifuge, washed with ethanol, and reused. The photocatalyst could be used up to 3 cycles with a loss of activity of 13%. However, this result indicates that it has good stability and recyclability.

Based on the molecular information obtained through literature, the photo-oxidation pathway of guaiacol over α-Fe_2O_3/TiO_2 with different molar ratios of β-CD was elucidated. According to the structure of guaiacol and the bond dissociation energy (BDE) calculated by Nowakowska and co-workers [57], the O—CH_3, O—H, and C—OCH_3 bond have dissociation energy as low as 58.1 kcal mol^{-1}, 87.1 kcal mol^{-1}, and 107.8 kcal mol^{-1}, respectively. These dissociations can be caused by different oxidation reactions of guaiacol and subsequent reactions of the formed radicals.

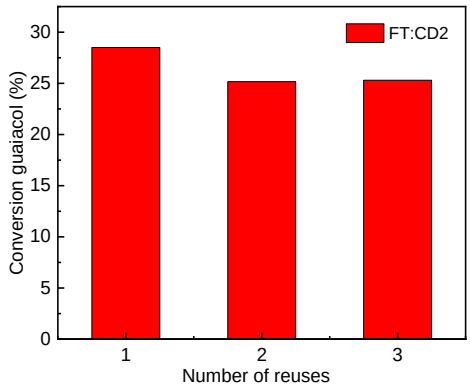

Fig. 6 The recycling of FT:CD2 for photocatalytic oxidation of guaiacol. Reaction conditions: $[guaiacol]_0$= 50 mg/L, $[photocatalyst]_0$= 1 g/L, reaction time = 300 min.

Fig. 8 shows the main pathways of guaiacol oxidation through reactive oxygen species as ·OH, $\cdot O_2$, $CH_3O\cdot$, and CHO· radicals. In all the irradiated photocatalytic system, the main product observed was *p*-benzoquinone (A1). This molecule can be further oxidized through H-abstraction in O—H promoted by $O_2^{\cdot-}/HO_2^{\cdot-}$ radical increase the formation of quinone intermediaries and weak bond break between C—OCH_3. The oxidation pathway is followed by the stabilization of intermediary state due to the *para* electrophilic addition of $O_2^{\cdot-}/HO_2^{\cdot-}$ radical to the aromatic ring, which can reorganize to form H_3O^+ and *p*-benzoquinone (A1). Furthermore, the reactants and products from all these reaction pathways can further undergo opening ring and fragmentation processes, resulting in the substantial formation of aldehyde, ketone, epoxide, and carboxylic acid initiated by successive oxidations of ·OH radicals, and finally to mineralization [58]. These over oxidations can affect the mass valance in aqueous media and were not quantified by current methods explaining the presence of other products in Fig. 6A. Other product observed was catechol (A2). Catechol is formed by the reaction between guaiacol and ·OH radical resulting in the break of weak bond among O-CH_3 group promoting the intermediate formation, followed by H-abstraction from the acid media, which results in the formation of catechol (A2)[59], [60]. The continuous oxidation of the catechol by ·OH radicals could produce pyrogallol (A3). However, under strong oxidant media produced by ·OH radicals the degradation or mineralization ways of pyrogallol are the most likely option [61]. Syringol (A4), and Vanillin (A5) can be formed from an intermediary derived from H-abstraction of guaiacol by ·OH radicals. These products were formed by the presence of oxidant species derived from guaiacol breaking such

as $CH_3O\cdot$, and $CHO\cdot$ radicals followed by electrophilic *ortho-para*-addition into aromatic ring of guaiacol.

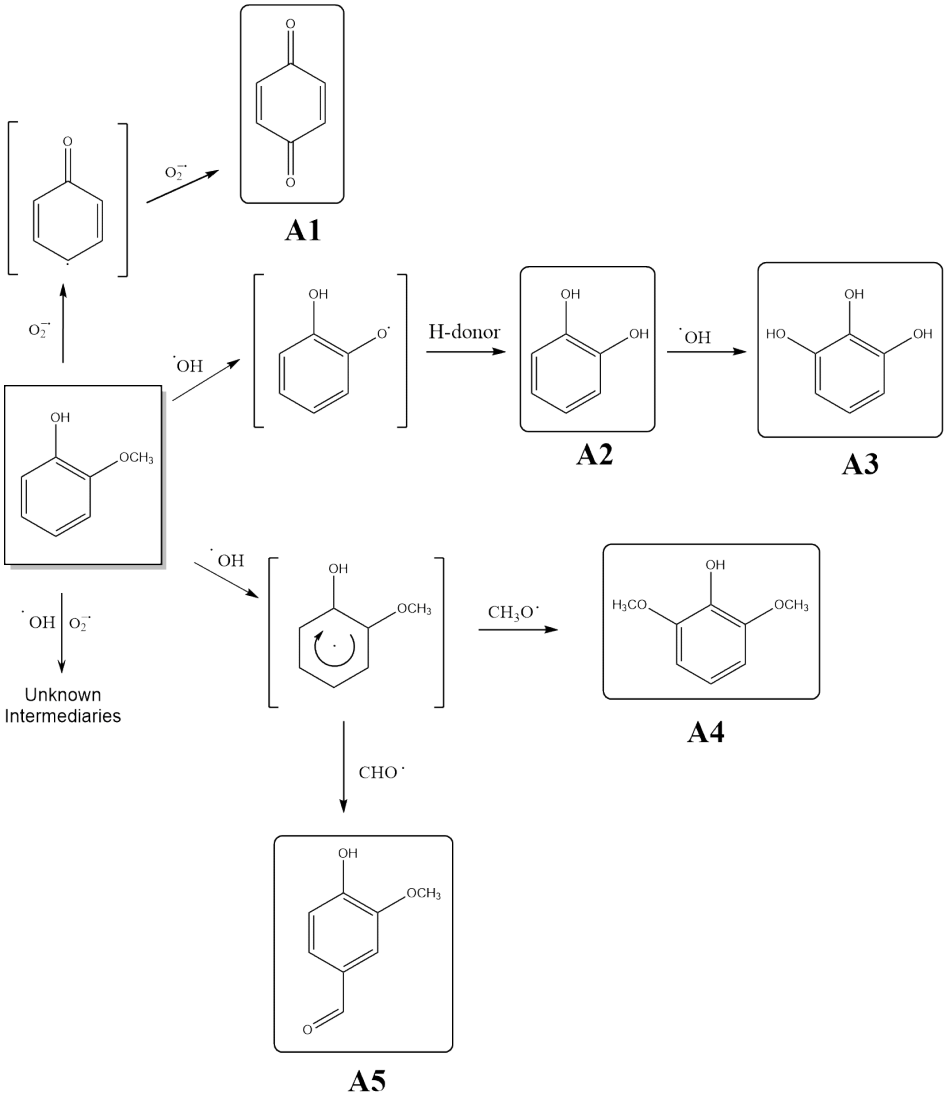

Fig. 7 Pathway of reaction of guaiacol in aqueous media when the solution is irradiated with UVA-visible light in presence of different photocatalysts.

Presence of β-CD over photocatalyst, decreased the amount of ·OH radicals as discussed above and therefore decreased over oxidation processes (such as ring opening) improving the mass balance and selectivity observed. Also, X. Zhang and coworkers [62] reported an increase on $O_2^{\cdot-}$ formation due to charge transfer between TiO_2 and β-CD, according to the reaction pathway proposed in Fig. 8, this will favor selective oxidation of guaiacol to *p*-benzoquinone in good agreement with obtained results.

4. Conclusion

In summary, efficient photocatalytic oxidization of guaiacol to *p*-benzoquinone has been developed under mild conditions by using a molar ratio of 1.0 mol of β-CD over α-Fe_2O_3/TiO_2. To determine the photocatalytic activity of the system, the conversion and selectivity, for the formation of *p*-benzoquinone were evaluated. These results show that a higher concentration of β-CD anchored to the photocatalyst surface allows an increase of selectivity on the photocatalytic oxidation of guaiacol. This was mainly due to the control in the formation of ·OH radicals promoted by the attachment LMCT complex between β-CD and semiconductor which was confirmed by EPR analysis in operando mode. Furthermore, the decrease of semiconductor band gap allowed better absorption of UVA-Visible radiation through heterojunction formation. FT:CD2, which presented the best results of photocatalytic activity, also showed to be stable after three uses, which is a highly desirable behavior for future industrial application. In this sense, this work provides an effective and mild approach for highly selective oxidation of biomass-derived feedstocks into high added-valuable compounds under ambient and greener conditions mediated by the use of β-CD. Confirming that photocatalysis has great potential in the field of biomass transformation.

Acknowledgements

The authors thank the funding from the Millennium Science Initiative of the Ministry of Economy, Development, and Tourism, grant Nuclei on Catalytic Processes towards Sustainable Chemistry (CSC), VRI Puente Project Nº 3913-556-81 at UC for financial support, DICYT-USACH, Fondequip EQM150101, and EQM160070 and PIA CCTE AFB 170007 projects.

Conflicts of interest

There are no conflicts to declare.

Notes and references

[1] D. S. Painter, “Burning Up: A Global History of Fossil Fuel Consumption,” *J. Interdiscip. Hist.*, vol. 50, no. 3, pp. 442–443, Nov. 2019, doi: 10.1162/jinh_r_01454.

[2] D. Shekhawat, J. J. Spivey, and D. A. Berry, *Fuel Cells: Technologies for Fuel Processing*. Elsevier, 2011.

[3] R. A. Sheldon, “Green and sustainable manufacture of chemicals from biomass: State of the art,” *Green Chem.*, vol. 16, no. 3, pp. 950–963, 2014, doi: 10.1039/c3gc41935e.

[4] S. H. Li, S. Liu, J. C. Colmenares, and Y. J. Xu, “A sustainable approach for lignin valorization by heterogeneous photocatalysis,” *Green Chem.*, vol. 18,

no. 3, pp. 594–607, 2016, doi: 10.1039/c5gc02109j.

[5] S. Gazi, “Valorization of wood biomass-lignin via selective bond scission: A minireview,” *Appl. Catal. B Environ.*, vol. 257, no. March, 2019, doi: 10.1016/j.apcatb.2019.117936.

[6] C. Liu, Y. Zhang, and X. Huang, “Study of guaiacol pyrolysis mechanism based on density function theory,” *Fuel Process. Technol.*, vol. 123, pp. 159–165, 2014, doi: 10.1016/j.fuproc.2014.01.002.

[7] L. I. Granone, F. Sieland, N. Zheng, R. Dillert, and D. W. Bahnemann, “Photocatalytic conversion of biomass into valuable products: A meaningful approach?,” *Green Chem.*, vol. 20, no. 6, pp. 1169–1192, 2018, doi: 10.1039/c7gc03522e.

[8] K. Chen, M. Cao, C. Ding, and X. Zheng, “A green approach for the synthesis of novel Ag3PO4/SnO2/porcine bone and its exploitation as a catalyst in the photodegradation of lignosulfonate into alkyl acids,” *RSC Adv.*, vol. 8, no. 47, pp. 26782–26792, 2018, doi: 10.1039/c8ra04962a.

[9] H. Zhang, Y. Wang, S. Shao, and R. Xiao, “Catalytic conversion of lignin pyrolysis model compound- guaiacol and its kinetic model including coke formation,” *Sci. Rep.*, vol. 6, no. November, pp. 1–10, 2016, doi: 10.1038/srep37513.

[10] A. M. Peiró, J. A. Ayllón, J. Peral, and X. Doménech, “TiO2-photocatalyzed degradation of phenol and ortho-substituted phenolic compounds,” *Appl. Catal. B Environ.*, vol. 30, no. 3–4, pp. 359–373, 2001, doi: 10.1016/S0926-3373(00)00248-4.

[11] L. I. Granone, F. Sieland, N. Zheng, R. Dillert, and D. W. Bahnemann, “Photocatalytic conversion of biomass into valuable products: A meaningful approach?,” *Green Chem.*, vol. 20, no. 6, pp. 1169–1192, 2018, doi: 10.1039/c7gc03522e.

[12] J. C. Colmenares and R. Luque, “Heterogeneous photocatalytic nanomaterials: Prospects and challenges in selective transformations of biomass-derived compounds,” *Chem. Soc. Rev.*, vol. 43, no. 3, pp. 765–778, 2014, doi: 10.1039/c3cs60262a.

[13] Y. Colmenares, J.C., Xu, *Heterogeneous Photocatalysis: From Fundamentals to Green Chemistry*. SPRINGER, 2016.

[14] S. J. A. Moniz, S. A. Shevlin, X. An, Z. X. Guo, and J. Tang, “Fe2O3-TiO2 nanocomposites for enhanced charge separation and photocatalytic activity,” *Chem. - A Eur. J.*, vol. 20, no. 47, pp. 15571–15579, 2014, doi: 10.1002/chem.201403489.

[15] A. Banisharif *et al.*, “Highly active Fe2O3-doped TiO2 photocatalyst for degradation of trichloroethylene in air under UV and visible light irradiation: Experimental and computational studies,” *Appl. Catal. B Environ.*, vol. 165, pp.

577 209–221, 2015, doi: 10.1016/j.apcatb.2014.10.023.

578 [16] S. C. Lee, H. O. Lintang, and L. Yuliati, “High photocatalytic activity of
579 Fe2O3/TiO2nanocomposites prepared by photodeposition for degradation of
580 2,4-dichlorophenoxyacetic acid,” *Beilstein J. Nanotechnol.*, vol. 8, no. 1, pp.
581 915–926, 2017, doi: 10.3762/bjnano.8.93.

582 [17] A. M. Abdel-Wahab, A. S. Al-Shirbini, O. Mohamed, and O. Nasr,
583 “Photocatalytic degradation of paracetamol over magnetic flower-like
584 TiO2/Fe2O3core-shell nanostructures,” *J. Photochem. Photobiol. A Chem.*,
585 vol. 347, pp. 186–198, 2017, doi: 10.1016/j.jphotochem.2017.07.030.

586 [18] X. Cao, S. Luo, C. Liu, and J. Chen, “Synthesis of Bentonite-Supported
587 Fe2O3-Doped TiO2 superstructures for highly promoted photocatalytic activity
588 and recyclability,” *Adv. Powder Technol.*, vol. 28, no. 3, pp. 993–999, 2017,
589 doi: 10.1016/j.apt.2017.01.003.

590 [19] H. Fu *et al.*, “A facile coating method to construct uniform porous α-
591 Fe2O3@TiO2 core-shell nanostructures with enhanced solar light
592 photocatalytic activity,” *Powder Technol.*, vol. 328, pp. 389–396, 2018, doi:
593 10.1016/j.powtec.2018.01.067.

594 [20] N. Sharma and A. Baldi, “Exploring versatile applications of cyclodextrins: An
595 overview,” *Drug Deliv.*, vol. 23, no. 3, pp. 739–757, 2016, doi:
596 10.3109/10717544.2014.938839.

597 [21] X. He, Z. Wu, Y. Xue, Z. Gao, and X. Yang, “Fabrication of interlayer β-CD/g-
598 C 3 N 4 @MoS 2 for highly enhanced photodegradation of glyphosate under
599 simulated sunlight irradiation,” *RSC Adv.*, vol. 9, no. 8, pp. 4635–4643, 2019,
600 doi: 10.1039/c8ra10190f.

601 [22] K. Liu, H. Fu, Y. Xie, L. Zhang, K. Pan, and W. Zhou, “Assembly of β-
602 Cyclodextrins Acting as Molecular Bricks onto Multiwall Carbon Nanotubes,”
603 *J. Phys. Chem. C*, vol. 112, no. 4, pp. 951–957, Jan. 2008, doi:
604 10.1021/jp0756754.

605 [23] C. J. Bae, S. Angappane, Y. Lee, J. Lee, K. An, and T. Hyeon, “Photocatalysis
606 of g–cyclodextrin-functionalised Fe3O4 nanoparticles for degrading Bisphenol
607 A in polluted waters,” *Environ. Chem.*, pp. 4–6, 2007, doi: 10.1063/1.2778758.

608 [24] M. Freitag and E. Galoppini, “Molecular host-guest complexes: Shielding of
609 guests on semiconductor surfaces,” *Energy Environ. Sci.*, vol. 4, no. 7, pp.
610 2482–2494, 2011, doi: 10.1039/c0ee00396d.

611 [25] H. M. C. Marques, “A review on cyclodextrin encapsulation of essential oils
612 and volatiles,” *Flavour Fragr. J.*, vol. 25, no. 5, pp. 313–326, 2010, doi:
613 10.1002/ffj.2019.

614 [26] R. L. Abarca, F. J. Rodríguez, A. Guarda, M. J. Galotto, and J. E. Bruna,
615 “Characterization of beta-cyclodextrin inclusion complexes containing an
616 essential oil component,” *Food Chem.*, vol. 196, pp. 968–975, 2016, doi:

10.1016/j.foodchem.2015.10.023.

[27] S. Ghosh-Mukerji, H. Haick, M. Schvartzman, and Y. Paz, “Selective photocatalysis by means of molecular recognition,” *J. Am. Chem. Soc.*, vol. 123, no. 43, pp. 10776–10777, 2001, doi: 10.1021/ja0117635.

[28] M. A. Lazar and W. A. Daoud, “Achieving selectivity in TiO2-based photocatalysis,” *RSC Adv.*, vol. 3, no. 13, pp. 4130–4140, 2013, doi: 10.1039/c2ra22665k.

[29] Daniel Chateigner *et al.*, “Crystallography Open Database.” http://www.crystallography.net/cod/ (accessed Apr. 10, 2021).

[30] J. E. Lohr, *Gusta v KortUm Reflectance Spectroscopy*. 1969.

[31] Q. Mei, F. Zhang, N. Wang, Y. Yang, R. Wu, and W. Wang, “TiO2/Fe2O3 heterostructures with enhanced photocatalytic reduction of Cr(vi) under visible light irradiation,” *RSC Adv.*, vol. 9, no. 39, pp. 22764–22771, 2019, doi: 10.1039/c9ra03531a.

[32] M. Lazzeri, A. Vittadini, and A. Selloni, “Structure and energetics of stoichiometric TiO2 anatase surfaces,” *Phys. Rev. B - Condens. Matter Mater. Phys.*, vol. 63, no. 15, pp. 1554091–1554099, 2001, doi: 10.1103/PhysRevB.63.155409.

[33] R. Hengerer, B. Bolliger, M. Erbudak, and M. Grätzel, “Structure and stability of the anatase TiO2 (101) and (001) surfaces,” *Surf. Sci.*, vol. 460, no. 1–3, pp. 162–169, 2000, doi: 10.1016/S0039-6028(00)00527-6.

[34] K. Sakurai and M. Mizusawa, “X-ray diffraction imaging of anatase and rutile,” *Anal. Chem.*, vol. 82, no. 9, pp. 3519–3522, 2010, doi: 10.1021/ac9024126.

[35] N. D. Johari, Z. M. Rosli, J. M. Juoi, and S. A. Yazid, “Comparison on the TiO2 crystalline phases deposited via dip and spin coating using green sol-gel route,” *J. Mater. Res. Technol.*, vol. 8, no. 2, pp. 2350–2358, 2019, doi: 10.1016/j.jmrt.2019.04.018.

[36] J. Zhang *et al.*, “Regulating photocatalytic selectivity of anatase TiO 2 with {101}, {001}, and {111} facets,” *J. Am. Ceram. Soc.*, vol. 97, no. 12, pp. 4005–4010, 2014, doi: 10.1111/jace.13187.

[37] L. X. Song, H. M. Wang, Y. Yang, and P. Xu, “Preparation and characterization of two solid supramolecular inclusion complexes of guaiacol with ß- And γ-cyclodextrin,” *Bull. Chem. Soc. Jpn.*, vol. 80, no. 11, pp. 2185–2195, 2007, doi: 10.1246/bcsj.80.2185.

[38] G. Lopes Colpani *et al.*, “Carboxymethyl-β-cyclodextrin functionalization of TiO2 doped with lanthanum: Characterization and enhancement of photocatalytic activity,” *Catal. Sci. Technol.*, vol. 8, no. 10, pp. 2636–2647, 2018, doi: 10.1039/c7cy02115a.

[39] M. E. Navgire, P. Gogoi, B. Mallesham, A. Rangaswamy, B. M. Reddy, and M.

K. Lande, “β-Cyclodextrin supported MoO3-CeO2 nanocomposite material as an efficient heterogeneous catalyst for degradation of phenol,” *RSC Adv.*, vol. 6, no. 34, pp. 28679–28687, 2016, doi: 10.1039/c5ra25966e.

[40] C. Di Valentin *et al.*, “N-doped TiO2: Theory and experiment,” *Chem. Phys.*, vol. 339, no. 1–3, pp. 44–56, 2007, doi: 10.1016/j.chemphys.2007.07.020.

[41] G. Wang, F. Wu, X. Zhang, M. Luo, and N. Deng, “Enhanced TiO2 photocatalytic degradation of bisphenol E by β-cyclodextrin in suspended solutions,” *J. Hazard. Mater.*, vol. 133, no. 1–3, pp. 85–91, 2006, doi: 10.1016/j.jhazmat.2005.09.058.

[42] J. Szejtli, “Introduction and general overview of cyclodextrin chemistry,” *Chem. Rev.*, vol. 98, no. 5, pp. 1743–1753, 1998, doi: 10.1021/cr970022c.

[43] M. Jaouadi, S. Hbaieb, H. Guedidi, L. Reinert, N. Amdouni, and L. Duclaux, “Preparation and characterization of carbons from β-cyclodextrin dehydration and from olive pomace activation and their application for boron adsorption,” *J. Saudi Chem. Soc.*, vol. 21, no. 7, pp. 822–829, Nov. 2017, doi: 10.1016/j.jscs.2016.01.001.

[44] M. Thommes *et al.*, “Physisorption of gases, with special reference to the evaluation of surface area and pore size distribution (IUPAC Technical Report),” *Pure Appl. Chem.*, vol. 87, no. 9–10, pp. 1051–1069, 2015, doi: 10.1515/pac-2014-1117.

[45] N. Attarchi, M. Montazer, and T. Toliyat, “Ag/TiO2/β-CD nano composite: Preparation and photo catalytic properties for methylene blue degradation,” *Appl. Catal. A Gen.*, vol. 467, pp. 107–116, 2013, doi: 10.1016/j.apcata.2013.07.018.

[46] A. Kaur, A. Umar, and S. K. Kansal, “Sunlight-driven photocatalytic degradation of non-steroidal anti-inflammatory drug based on TiO2 quantum dots,” *J. Colloid Interface Sci.*, vol. 459, pp. 257–263, 2015, doi: 10.1016/j.jcis.2015.08.010.

[47] R. Velmurugan, B. Krishnakumar, B. Subash, and M. Swaminathan, “Preparation and characterization of carbon nanoparticles loaded TiO 2 and its catalytic activity driven by natural sunlight,” *Sol. Energy Mater. Sol. Cells*, vol. 108, pp. 205–212, 2013, doi: 10.1016/j.solmat.2012.09.018.

[48] J. Kochany and J. R. Bolton, “Mechanism of photodegradation of aqueous organic pollutants. 1. EPR spin-trapping technique for the determination of hydroxyl radical rate constants in the photooxidation of chlorophenols following the photolysis of hydrogen peroxide,” *J. Phys. Chem.*, vol. 95, no. 13, pp. 5116–5120, Jun. 1991, doi: 10.1021/j100166a039.

[49] G. R. Buettner, “Spin Trapping - Electron-Spin-Resonance Parameters of Spin Adducts,” *Free Radic. Bio. Med.*, vol. 3, no. 4, pp. 259–303, 1987, doi: 10.1016/s0891-5849(87)80033-3.

[50] Q. Sun, W. Leng, Z. Li, and Y. Xu, “Effect of surface Fe 2O 3 clusters on the photocatalytic activity of TiO 2 for phenol degradation in water,” *J. Hazard. Mater.*, vol. 229–230, pp. 224–232, 2012, doi: 10.1016/j.jhazmat.2012.05.098.

[51] P. Lu, F. Wu, and N. Deng, “Enhancement of TiO2 photocatalytic redox ability by β-cyclodextrin in suspended solutions,” *Appl. Catal. B Environ.*, vol. 53, no. 2, pp. 87–93, 2004, doi: 10.1016/j.apcatb.2004.04.016.

[52] G. Zhang, G. Kim, and W. Choi, “Visible light driven photocatalysis mediated via ligand-to-metal charge transfer (LMCT): An alternative approach to solar activation of titania,” *Energy Environ. Sci.*, vol. 7, no. 3, pp. 954–966, 2014, doi: 10.1039/c3ee43147a.

[53] X. Zhang, X. Li, and N. Deng, “Enhanced and selective degradation of pollutants over cyclodextrin/TiO 2 under visible light irradiation,” *Ind. Eng. Chem. Res.*, vol. 51, no. 2, pp. 704–709, 2012, doi: 10.1021/ie201694v.

[54] B. Rajbanshi *et al.*, “Study to Probe Subsistence of Host-Guest Inclusion Complexes of α and β-Cyclodextrins with Biologically Potent Drugs for Safety Regulatory Dischargement,” *Sci. Rep.*, vol. 8, no. 1, pp. 1–20, 2018, doi: 10.1038/s41598-018-31373-x.

[55] G. Astray, J. C. Mejuto, J. Morales, R. Rial-Otero, and J. Simal-Gándara, “Factors controlling flavors binding constants to cyclodextrins and their applications in foods,” *Food Res. Int.*, vol. 43, no. 4, pp. 1212–1218, 2010, doi: 10.1016/j.foodres.2010.02.017.

[56] S. A. Wildman and G. M. Crippen, “Prediction of physicochemical parameters by atomic contributions,” *J. Chem. Inf. Comput. Sci.*, vol. 39, no. 5, pp. 868–873, 1999, doi: 10.1021/ci990307l.

[57] M. Nowakowska, O. Herbinet, A. Dufour, and P. A. Glaude, “Kinetic Study of the Pyrolysis and Oxidation of Guaiacol,” *J. Phys. Chem. A*, vol. 122, no. 39, pp. 7894–7909, 2018, doi: 10.1021/acs.jpca.8b06301.

[58] D. Zhang, B. Sun, L. Duan, Y. Tao, A. Xu, and X. Li, “Photooxidation of Guaiacol to Organic Acids with Hydrogen Peroxide by Microwave Discharge Electrodeless Lamps,” *Chem. Eng. Technol.*, vol. 39, no. 1, pp. 97–101, 2016, doi: 10.1002/ceat.201500251.

[59] S. Karthikeyan *et al.*, “Size-Dependent Visible Light Photocatalytic Performance of Cu2O Nanocubes,” *ChemCatChem*, vol. 10, no. 16, pp. 3554–3563, 2018, doi: 10.1002/cctc.201800439.

[60] M. Asmadi, H. Kawamoto, and S. Saka, “The effects of combining guaiacol and syringol on their pyrolysis,” *Holzforschung*, vol. 66, no. 3, pp. 323–330, 2012, doi: 10.1515/hf.2011.165.

[61] Y. Samet, I. Wali, and R. Abdelhédi, “Kinetic degradation of the pollutant guaiacol by dark Fenton and solar photo-Fenton processes,” *Environ. Sci. Pollut. Res.*, vol. 18, no. 9, pp. 1497–1507, 2011, doi: 10.1007/s11356-011-

736 0514-4.

737 [62] X. Zhang, X. Li, and N. Deng, “Enhanced and selective degradation of
738 pollutants over cyclodextrin/TiO 2 under visible light irradiation,” *Ind. Eng.*
739 *Chem. Res.*, vol. 51, no. 2, pp. 704–709, 2012, doi: 10.1021/ie201694v.

740